Dark Matter Halo Density Profile Calibration

Titus N. Nde (Computing Ph.D)
Boise State University
Boise, ID 83725
titusnyarkonde@u.boisestate.edu

August 29, 2022

Abstract

In this synthesis, we reviewed the literature on halo density calibration. Several years of research have been conducted to understand dark matter but it still remains a mystery to Cosmologists. Despite many efforts, there still remain significant gaps in the literature. The ultimate goal is to reconcile dark matter theories (which include fitting functions and simulations) with observations. This will help us obtain an accurate and thorough understanding of the dark matter halo density profiles, which will in turn help us understand the formation of cosmic structure. New halo properties have been detected in simulations and observations but they are still not well understood. Analytic fitting functions such as NFW and Einasto profiles have also been shown to perform poorly under several conditions. We do not know yet if new physics can help us understand the mysterious dark matter but probing dark matter halos remains a good approach. We identified gaps in the literature and suggested solutions to some of them. Specifically, we demonstrated how machine learning can help us obtain more accurate predictions than analytic models and also estimate error bars on these predictions. Finally, we presented a computing artifact on uncertainty quantification. The computing artifact is available in a public GitHub repository via this link.

1 Introduction

A dark matter halo is a hypothesized region dominated by gravitationally bound invisible matter in which galaxies, galaxy clusters, and groups form and live. Dark matter halos are fundamental building blocks of large-scale structures and the cosmic web in general. They stretch beyond the visible region of galaxies and galaxy clusters. They are also dark-matter-dominated structures whose properties help to understand the nature of the mysterious dark matter, galaxy and galaxy cluster formation and evolution, and cosmology in general. According to the Lambda Cold Dark Matter (hereafter ΛCDM) model, our universe is dominated by dark energy ($\sim$ 68%) and dark matter ($\sim$ 27% and $\sim$ 85% of all matter in our Universe). Baryons are ordinary matter — elements in the periodic table. They constitute only $\sim$ 5% of the Universe but $\sim$ 15% of the total matter in the Universe. Note that the ΛCDM model is referred to as the standard model of cosmology and Λ denotes dark energy. Also, the ΛCDM cosmology is dominated by dark energy — this discovery was made in the year 1998 and has revolutionalized research in astronomy.

We do not yet understand perfectly the nature of dark matter. As a matter of fact, Cosmologists know much about what it is not rather than what it is. Dark matter is attractive and accounts for structure formation in our Universe. On the other hand, dark energy is repulsive and accounts for cosmic acceleration, from which its existence was also inferred.

Understanding the density profiles of ΛCDM halos is one of the interesting probes to cluster cosmology and dark matter. Density profiles offer a promising avenue to deduce dark matter characteristics. Galaxy clusters are the largest objects bound by gravity in the cosmos. Dark matter halo formation is complex but their density profiles help to explain the mass distribution in these gravitationally bound structures and give a practical way to link theory to observations from galaxy surveys (Fielder et al., 2020; Nishimichi et al., 2019; Shin et al., 2021; Diemer, 2022). We cannot directly observe cluster mass; however, it can be derived from observable properties such as cluster richness, velocity dispersion, stellar mass, gravitational lensing, X-ray emission, and Sunyaev-Zeldovich (SZ) effect (Salcedo et al., 2019).

Gravitational lensing is the bending of light traveling from a source galaxies to an observer due to the presence of a galaxy cluster acting as a lens between the observer and the source galaxies. If the observer, the lens, and the source are perfectly positioned in a straight line, then the observer will see the source as a ring around the lens. Sometimes the observer might even see multiple images of the same source galaxy. This is called strong gravitational lensing. If the three are not absolutely positioned in a straight line, by any little deviation, then the observer will see the source galaxy appearing as an arc. This is called weak gravitational lensing and it is the most predominant form of gravitational lensing in the Universe. We can measure the mass distribution and halo density profiles via weak lensing (hereafter WL) methods like the so-called concentration-mass and richness-mass relations (Henson et al., 2017; McClintock et al., 2019; Shin et al., 2021). WL mass estimation is the most robust of all mass estimation techniques available in the literature McClintock et al. (2019). Dark-matter-only simulations typically use WL measurements.

Also, we do not observe halos directly but we can deduce their characteristics such as mass distribution and potential due to gravity from WL. Hence, serves as an avenue to probe halo density profiles (Shin et al., 2021). We can also derive the distribution of source galaxies from photometric redshift.

Fig. 1 shows the simulation of a massive halo. Bright spots in the cosmic web are dark matter halos connected by filaments. Filaments are also dark-matter-dominated structures. Some low-mass halos live inside filaments. The dark regions are voids — empty or devoid of matter.

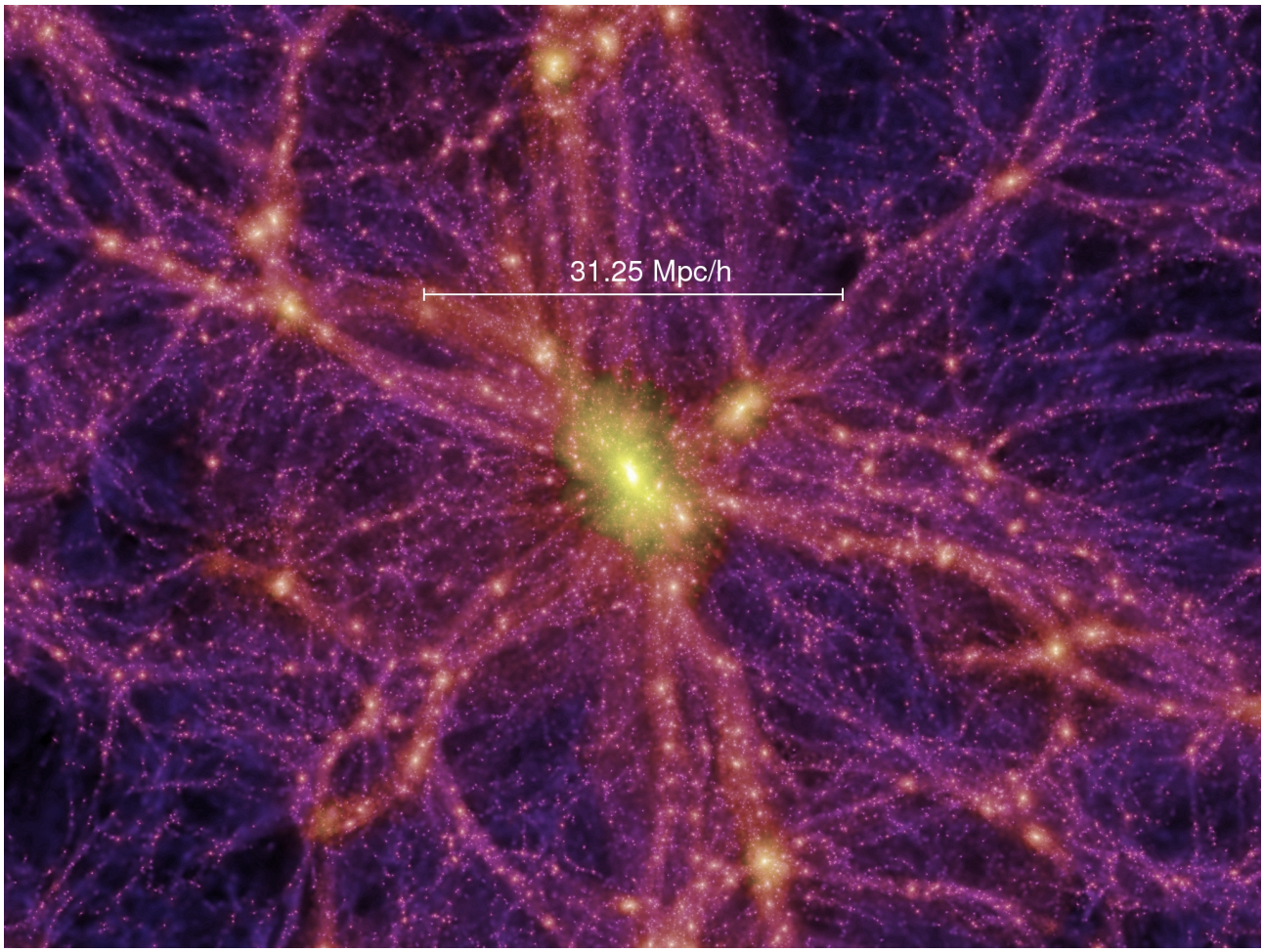

Figure 1: Image of a ΛCDM halo from a simulation. This is a zoom into a really tiny portion of the cosmic web. The distance to travel across the image from left to right is about 400 light years. The redshift of the halo is 0. The brightest regions are halos connected by filaments. Filaments are also dark-matter-dominated structures. Some low-mass halos live inside filaments. The dark regions are voids — empty or devoid of matter. (Credit: The Millennium Simulation Project.)

Dark matter was inferred from gas and stellar motions in galaxies. For instance, the amount of luminous matter in spiral galaxies cannot explain the observed rotation curves of stars within them. Also, galaxies in

clusters or groups would move away from each other if clusters or groups were made of only luminous matter. This is because the galaxies are moving with very high velocities, and luminous matter alone cannot provide strong enough gravity to hold the galaxies together.

Interestingly, research findings in cosmology are evolving fast. This is because more data is being gathered from several astronomical surveys. Scientists are building sophisticated telescopes to collect extensive high-quality data. As we look further in space, the farther we can see into earlier in cosmic time. This means we can observe events that took place from the very beginning of our Universe. Photons from some of these events have not yet traveled to us. Thus, we are moving from an almost purely theoretical phase to an era of vast high-quality data availability. Studies have found inaccurate predictions from analytic models existing in the literature (Dutton & Macciò, 2014). Also see Fig. 2.

In Fig. 2, we plot the DK14, NFW, and Einasto profiles vs a halo simulated from the Buzzard N-Body simulation. We notice that all three profiles do not capture the detailed shape of the halo. Only the logarithmic slope of the DK14 profiles shows the presence of a splashback feature. Also, we can only notice differences between NFW and Einasto profiles at small and large radii.

The analytic models, as well as simulations, are cosmology-dependent. However, differences in cosmology might result in significant differences among simulations and predictions from analytic models. It becomes necessary to resolve these differences between cosmologies. Active research is being conducted in this area. ΛCDM halo density profile is one of the areas that will benefit from this. The ultimate end goal is to accurately calibrate halo density profiles as a probe to understand dark matter's nature and characteristics. The idea is to use observational data to probe and redefine our understanding of existing theories. We can also use observational results to set high accuracy constraints on existing theories, analytic models, and simulations Diemer & Kravtsov (2014); Shin et al. (2021); Diemer (2022). Much research has been conducted with varying objectives with the sole aim of accurately calibrating ΛCDM halo density profiles. See Table 1 for the major objectives of the four main seed papers considered in this synthesis.

Another probe to bridging the gap between theory and observation is new physics. Perhaps, a discovery of new form(s) of dark matter might change our understanding of the Universe and its evolution. Also, we may have to redefine and modify our understanding, as well as existing theories, of gravity (such as rotation in orbits) on cosmological scales to be able to bridge this gap. Only a few cosmological studies focus on new physics in the literature. However, this remains an active area of research.

This synthesis considers the following seed papers:

- **Paper I:** Dependence of the outer profiles of halos on their mass accretion rate (Diemer & Kravtsov, 2014)
- **Paper II:** The mass and galaxy distribution around SZ-selected clusters (Shin et al., 2021)
- **Paper III:** A dynamics-based density profile for dark halos – I. Algorithm and basic results (Diemer, 2022)
- **Paper IV:** The impact of baryons on massive galaxy clusters: halo structure and cluster mass estimates (Henson et al., 2017)

The remainder of this synthesis is organized as follows. Section 2 talks about how differences in cosmologies impact theories and simulation, Section 3 introduces some important analytic models available in the literature, Section 4 talks about the current state of research on dark matter halo density calibrating, and Section 5 introduces a machine learning approach for dark matter halo density calibration. Finally, the summary and conclusions are presented in Section 6.

2 Cosmology, simulations, and terminologies

In this Section, we explore briefly how differences in results obtained from different astronomical surveys impact cosmological simulations. We also give reasons why there is a need to resolve these significant differences.

2.1 Cosmological results

cosmology refers to the study of the origin, nature, and evolution of the Universe. However, in this synthesis when we say cosmology, we are actually referring to the set of parameters describing the evolution and state of our Universe at the current epoch. Different astronomical surveys were conducted to derive these parameters. They help us study various properties of the evolution of our Universe by fitting cosmological parameters to

Table 1: Summary of papers. This table gives a high-level summary of the seed papers in this synthesis.

Paper	Objective	Support	Analysis	Result	Implication
Paper I	Measure density profiles' dependence on mass accretion rate, focusing on the outer region	N-body simulation. NFW and Einasto profiles poorly fit outer density profiles	Propose a new analytic model as a function of peak height and mass accretion rate	Detects the splashback feature for the first time in N-body simulations	The splashback feature should be detectable observationally in future weak lensing analyses
Paper II	Measure density profiles for both inner and outer regions	Observational data from ACTDR5[a] and DESY3[b]. SZ-selected data suffer less systematic effects	Use HOD[c] and a modified form of DK14 profile with 2PT[d] to calibrate density profiles	Detects the splashback feature in SZ[e]-selected clusters for the first time	We are yet to understand the mass distribution around the splashback feature
Paper III	Understand the structure between the orbiting and infalling terms and beyond	N-Body simulations. We do not understand the mass distribution around the splashback term	Dynamically disentangle orbiting and infalling matter and model them separately	Orbiting regime show dependence on different fundamental spatial scales	We cannot model density profiles with single-scale models like NFW and Einasto
Paper IV	Measure the impact of baryons on the density profiles of high-mass halos	Hydrodynamic simulations. Ignoring baryons leads to systematic bias in mass estimation	Uses NFW and Einasto profiles to fit the data. Measured WL[f] and hydrostatic bias for mass calibration	Minor baryonic effect on the WL mass estimates of high-mass clusters and density profiles at large radii	Baryonic effect remains uncertain in high-mass halos due to limited sample sizes and high computational cost.

[a]ACTDR5: Atacama Cosmology Telescope Data Release 5
[b]DESY3: Dark Energy Survey Year 3 results
[c]HOD: Halo Occupation Distribution
[d]2PT: Second order perturbation theory
[e]SZ: Sunyaev-Zeldovich
[f]WL: weak lensing

observational results. They also help us set constraints on cosmological simulations. Some of the landmark cosmologies usually adopted in the literature include Wilkinson Microwave Anisotropy Probe (WMAP - Komatsu et al. (2011)) and Planck (Planck Collaboration et al., 2014). However, different astronomical surveys result in different values for these sets of parameters. Sometimes these discrepancies become highly statistically significant such that we can no longer neglect them. Two salient examples are the so-called Hubble tension and the σ_8 tension. Interestingly, the same astronomical survey usually results in slightly different values for these parameters from year to year. We do not know which cosmology represents our Universe best. To settle these discrepancies we need careful control of observational systematics. This will also help to set high accuracy constraints in models and simulations. Table 2 shows a brief overview of the discrepancies that exist between cosmologies. This table shows the most commonly adopted cosmological parameters for the past two decades. The Einstein-de Sitter cosmology is ruled out but is of theoretical interest since it is scale-free.

2.2 Cosmological simulations

Simulations help us understand the evolution of our Universe from a theoretical perspective. N-body simulations and hydrodynamic simulations are the two major types of cosmological simulations available in the literature. However, these simulations are cosmology-dependent. Hence, different simulations (even those of the same kind) might result in significantly different halo properties. This means that predictions based on these simulations are also cosmology-dependent. Below we present the two major types of simulations in the literature.

Table 2: Cosmological parameters from different astronomical surveys. The table shows the present-day values of the various cosmological parameters describing our Universe as measured from different astronomical surveys (except the Einstein-de Sitter cosmology). The Einstein-de Sitter cosmology is a universe made of 100% dark matter. This universe is not realistic because structure formation is self-similar over cosmic time scales, but it can be a good proxy for the ΛCDM cosmologies under certain conditions. For details on these parameters from the different astronomical surveys, see (Spergel et al., 2003; Komatsu et al., 2011; Planck Collaboration et al., 2014, 2020). The Wilkinson Microwave Anisotropy Probe (hereafter WMAP) and Planck results are based on Λ-dominated cosmologies.

cosmology	$\Omega_{m,0}{}^a$	h^b	$\sigma_8{}^c$	$n_s{}^d$
Einstein-de Sitter	1.0000	0.7000	0.8200	1.0000
WMAP1 (2003)	0.2700±0.04	0.7200±0.05	0.9000±0.1	0.9900±0.04
WMAP7 (2011)	0.2743±0.007	0.7020±0.014	0.8160±0.024	0.9680±0.012
Planck 2018	0.3111±0.0056	0.6766±0.0042	0.8102±0.006	0.9665±0.0038

[a]Matter density parameter
[b]Hubble constant
[c]Density fluctuation
[d]Scalar spectral index

N-body simulations are dark-matter-only simulations. They assume dark matter halos are made of only dark matter particles. This assumption is not accurate but this simulation yields reasonably good result.N-body Simulations are widely used in studies involving dark matter. The Millennium simulation (Springel et al., 2005) is an example of N-body simulation.

Unlike N-body simulations, hydrodynamic simulations account for the contribution of baryons to the mass distribution of dark matter halos. There is a systematic bias toward ignoring baryons and modeling halo density profiles as though they are dark-matter-only structures (Henson et al., 2017; Cromer et al., 2021). Hydrodynamic simulations also tend to produce more spherical and centrally concentrated halos than their dark-matter-only counterparts(Henson et al., 2017). However, the baryonic processes are not very well understood. Hydrodynamic simulations are computationally expensive because simulating the baryonic effect requires much higher resolutions than gravity.

Baryons dominate halo centers, but their dominance decreases as we move farther from the halo center. There are two major concerns here: On one hand, it is not yet well understood how dark matter is distributed near the halo center, where baryons dominate. On the other hand, it is not yet well understood how baryonic matter is distributed at large radii, where dark matter dominates (Henson et al., 2017; Shin et al., 2021). Hydrodynamic simulations are so important because they have the potential of providing answers to some of these key cosmological quests. Some examples of hydrodynamic simulations available in the literature include BAHAMAS (McCarthy et al., 2017) and MACSIS (Barnes et al., 2017) hydrodynamic simulations.

2.3 Halo properties and terminologies

Here we briefly explain some halo properties and terminologies to help the reader easily understand the content of this synthesis.

Redshift: This is the increase in wavelength of photons from luminous bodies as a result of the expansion of the Universe. The stretch in wavelength leads to a drop in frequency as well as photon energy. Redshift is typically used as a measure of distance to luminous bodies. Those farther away have higher redshift.

Halo radius: This is the radius within which the halo mass is defined. For instance, R_{200m} is the radius that contains on average 200 times the mean matter density of the Universe. M_{200m} is the corresponding mass contained within the sphere of radius R_{200m}. The same definitions can be given to R_{200c} and M_{200c} in terms of the critical density of the Universe, and R_{vir} and M_{vir} in terms of the varying virial overdensity.

Halo boundary: This is the largest orbit of matter gravitationally bound to the halo center. Any of the radial definitions, R_X, can be used to define a halo boundary with corresponding mass M_X. The region within $r \lesssim R_X$ is the inner region while the region beyond that, $r \gtrsim R_X$, constitutes the outer region of the halo (Diemer, 2022).

1-halo term: This refers to the inner region, $r \lesssim R_X$, of halos. It is so-called because it refers to contributions from matter within the same host halo. This region is dominated by gravitationally bound (orbiting) matter. It is also referred to as the orbiting term.

2-halo term: This refers to the region beyond the 1-halo term, $r \gtrsim R_X$. It is used to describe significant

contributions a halo receive from the mass of neighboring massive structures.
Infalling term: The outer region, $r \gtrsim R_X$, of a halo, is dominated by matter falling into it for the first time. This is called infalling matter or the infalling term. Infalling matter does not belong to a neighboring halo, unlike the 2-halo term. Infalling matter is gravitationally unbound (Diemer, 2022).
Splashback feature/region: This refers to a region of steep slope between the inner and outer regions of a halo. The splashback feature is also referred to as the transition region. This is where the orbiting term switches dominance with the infalling term as we move into the outer region. The radius at which the slope is steepest is called the **splashback radius**, often denoted as R_{sp}. The splashback radius can also be used to define a physically significant halo boundary. Diemer & Kravtsov (2014) adopted this definition for the halo boundary. See Fig. 3.
Truncation radius: This is the radius at which the slope of the density profile of the orbiting term truncates/drops sharply, often denoted as r_t. It is often used interchangeably as the splashback radius; however, Diemer (2022) reveals that the two are not exactly the same. Hence, we can only use r_t as a reasonable proxy for R_{sp}. See Fig. 2 and 3.
Scale radius: It is the radius at which the slope of the density profile is equal to -2, often denoted as r_s or r_{-2}. It is the ratio of R_X and the concentration parameter. Both NFW and Einasto profiles are scaled by only r_s (Diemer & Kravtsov, 2014; Fielder et al., 2020).
Concentration: This is the degree to which the halo mass is dense towards the halo center. It is defined by R_X/r_s. The concentration parameter is dimensionless.
Richness: It is historically defined as the number of galaxies belonging to a cluster or halo. Modern cluster finders usually use the sum of membership probabilities of galaxies belonging to a certain galaxy cluster or halo. **Mass accretion rate:** This is the rate at which a halo accumulates mass. A halo can accumulate mass via means like infalling and mergers (halos merging into one). Diemer & Kravtsov (2014) show that density profiles are sensitive to the total mass accretion rate rather than an instantaneous mass accretion via major mergers. They also show that high-mass halos have a higher mass accretion rate and vice versa. Also, halo masses pseudo-evolve due to changes in the definition of its radius (R_X) and expansion of the Universe (Diemer et al., 2013).
Peak height: This is also a dimensionless parameter. It makes the halo density profile universal and allows for mass comparison across redshift and cosmology. With peak height, we can compare halo masses across different redshifts. It is a function of mass and redshift.
Satellite or subhalo: This refers to a halo that lies within R_X of another halo called the host or parent halo. Parent halos are also called isolated halos.
Critical density: This refers to the matter density that keeps the curvature of our Universe flat.

3 Analytic fitting functions for density profiles

A density profile is a series of density estimates calibrated as a function of radial distance to the halo center. This section introduces some analytic fitting equations for halo density profiles. Specifically, Subsection 3.1 gives an overview of some 3-dimensional fitting equations while Subsection 3.2 introduces the 2-dimensional density profile.

3.1 3D density profiles

Many analytic models have been developed in the literature to calibrate halo density profiles. Given their theoretical foundations, these analytic models are cosmology-dependent. However, they serve as great tools for probing and improving our understanding of the characteristics of the mysterious dark matter. The Navarro-Frenk-White (hereafter NFW) density profile developed by Navarro et al. (1996, 1997) is given as:

$$\rho(r) = \frac{\rho_{crit}\delta_{crit}}{\frac{r}{r_s}\left(1+\frac{r}{r_s}\right)^2} \tag{1}$$

where $\rho(r)$ is the halo density, r is the distance from the halo center, $r_s = \frac{R_{200}}{c}$ is the characteristic or scale radius, ρ_{crit} is the critical density of the Universe, and δ_{crit} is the characteristic overdensity. The scale density, ρ_s, is usually used to replace $\rho_{crit}\delta_{crit}$.

The Einasto fitting function developed by Einasto (1965) is given as:

$$\rho(r) = \rho_s \exp\left(-\frac{2}{\alpha}\left[\left(\frac{r}{r_s}\right)^{\alpha} - 1\right]\right). \tag{2}$$

The major difference between the NFW and Einasto profiles is seen at large and small radii (see Fig. 2). The steepening term, α, controls the slope and thus determines the level of decline in the Einasto profile. The bigger the value of α, the steeper the slope of the Einasto profile. It is found to be a function of the dimensionless peak height parameter in Gao et al. (2008) as $\alpha(v) = 0.155 + 0.0095\nu^2$.

NFW and Einasto profiles are among the most popular analytic fitting functions in the literature despite some significant drawbacks. They are particularly good for fitting the inner density profiles, $r \lesssim R_{vir}$, of halos. Beyond this radii, they poorly calibrate the density profiles Diemer & Kravtsov (2014); Shin et al. (2019); Diemer (2022).

The DK14 profile developed by Diemer & Kravtsov (2014), is an extension to the Einasto profile. It introduces a new term describing the outer profile of halos. Other studies that precede Diemer & Kravtsov (2014) developed analytic models to describe the outer density profiles of halos. The idea is to prevent the analytic density profile models from approaching zero in the outer regions, $r \gtrsim R_{vir}$. This behavior is typical of the NFW profile for instance. The analytic fitting formulae proposed for describing the outer regions of halos generally tend to the mean matter density at sufficiently large radii (Diemer & Kravtsov, 2014). Prada et al. (2006) suggests adding the mean matter density of the universe to the Einasto profile to describe the outer region; meanwhile, Tavio et al. (2008) rather propose an improvement to the NFW profile. Hayashi & White (2008) also propose an approach to fit the 1-halo term by NFW or Einasto profile, and the 2-halo term by a modified form of the linear mass auto-correlation function. The maximum between the two is adopted in the transition region. This method works pretty well but there is no theoretical justification to explain why it works. On the other hand, Oguri & Hamana (2011) propose adopting the sum of the 1-halo and 2-halo terms to calibrate density profiles. However, their approach has been detected to overestimate the transition region. Despite having all these fitting formulae in the literature, the DK14 profile has gained much attention due to its flexibility in describing the variations in the outer density profiles of ΛCDM halos. The DK14 profile is given as:

$$\rho(r) = \rho_{inner} \times f_{trans} + \rho_{outer} \tag{3}$$

$$\rho(r) = \rho_s \exp\left(-\frac{2}{\alpha}\left[\left(\frac{r}{r_s}\right)^{\alpha} - 1\right]\right) \times \left[1 + \left(\frac{r}{r_t}\right)^{\beta}\right]^{-\frac{\gamma}{\beta}} + \rho_m \left[b_e \left(\frac{r}{5R_{200}}\right)^{-s_e} + 1\right]; \quad s_e > 0. \tag{4}$$

This profile tends to the Einasto profile when we omit the outer term and set γ to 0. The outer term, ρ_{outer}, is characterized by a power law plus the mean density of the Universe, ρ_m. r_t is the truncation radius and the f_{trans} term helps to explain how the halo profile deepens around the truncation radius. Also, at r_t the slope of the DK14 profile begins to decline more sharply than the Einasto profile. γ is the term that determines the asymptotic negative slope; it defines how the DK14 profile deepens at, $r \approx R_{200m}$, and β defines the sharpness of the change in slope (Diemer & Kravtsov, 2014). Setting $s_e > 0$ constraints the outer term, ρ_{outer}, so that the contribution from infalling matter does not surpass that of the orbiting matter in the inner region, ρ_{inner}. This is because setting $s_e > 0$ means setting an upper bound on the highest value ρ_{outer} can assume (Diemer & Kravtsov, 2014; Shin et al., 2021). According to Diemer & Kravtsov (2014), the profile at sufficiently large radii might not stick to a power law or tend to the mean matter density of the universe. For instance, it will tend to a form consistent with the matter correlation function at $r \gtrsim 9R_{vir}$. Interestingly, it is also possible to parameterize the outer density profile with infalling matter which relies much on the total mass accretion rate and the environment for fast and slowly accreting ΛCDM halos, respectively. See Diemer (2022) for more details on how to model the outer density profile of halos with infalling matter. Also, see Hayashi & White (2008) and Appendix A.1 of Diemer & Kravtsov (2014) for details on how to link the density profile of the outer regions of halos to the 2-halo term.

The DK14 fitting equation is a function of peak height or mass accretion rate. For low peak height halos, NFW and Einasto reasonably calibrate the density profiles but they are unable to capture the sharp decline in slope in the density profiles of high peak height halos around the truncation radius (Diemer & Kravtsov, 2014).

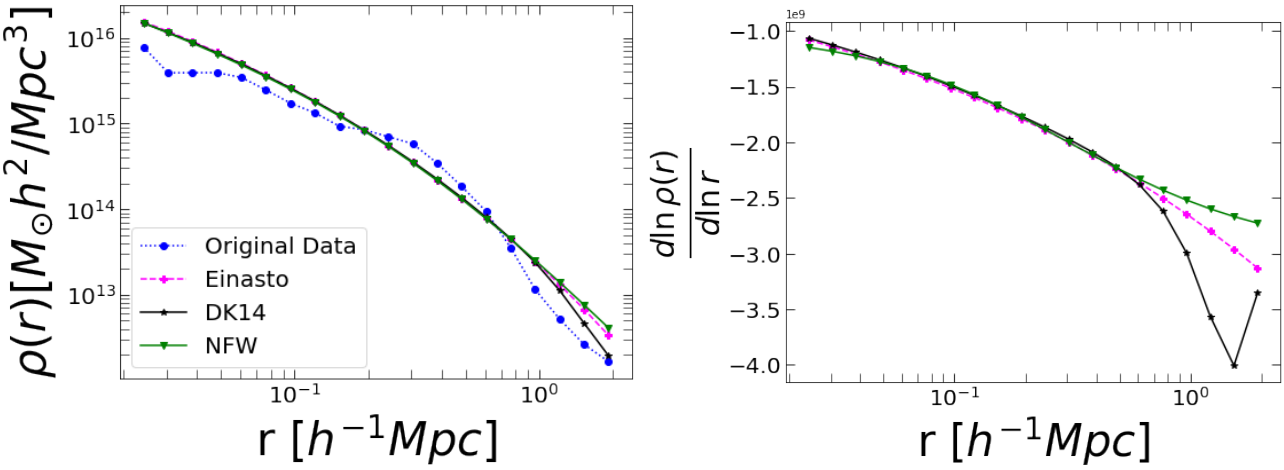

Figure 2: *Left panel:* 3-dimensional DK14, NFW, and Einasto density profiles vs a halo from the Buzzard N-body simulation. We notice that the analytic models are not able to capture the detailed shape of the actual halo density profile. The halo plotted above has the following properties; $M_{vir} = 3.9 \times 10^{14}, z = 0.39, c = 3.97, R_{vir} = 1.21$, and $= 0.24$. We adopted the default optimal parameters in COLOSSUS, $\beta = 4$ and $\gamma = 8$, for the DK14 profile. *Right panel:* The logarithmic slope of the analytic density profiles. The clear difference between the Einasto and NFW profiles can be seen at small and large radii, and the point at which the DK14 profile begins to steepen more than the Einasto profile is the truncation radius, r_t. There is no difference between Einasto and DK14 profiles at $r \lesssim r_t$. We can only see the splashback feature from the slope of the DK14 profile.

3.2 2D density profile and gravitational lensing

We can obtain the 2D density profile by integrating the 3D density profile over the line-of-sight distance, l. The 2D density, Σ, is so important because observationally we see the sky in 2D. Therefore, we can only calibrate density by surface area rather than volume. 3D densities are only directly available in simulations. Moreover, the 3D density fitting equations also assume dark matter halos are spherically symmetric; though this assumption is often inaccurate (Mandelbaum et al., 2008; Chang et al., 2018; Cromer et al., 2021; Shin et al., 2021). The 2D density equation is given as follows:

$$\Sigma(R) = \int_{-l_{max}}^{l_{max}} \rho\left(r = \sqrt{R^2 + l^2}\right) dl, \tag{5}$$

where l is the line-of-sight distance to the galaxy cluster or halo and R is the projected halo radius. Note that the surface density, Σ, is also related to the magnification effect. The magnification effect is a consequence of WL, which makes a galaxy or galaxy cluster appear brighter and bigger than its actual brightness and size, respectively. However, it is difficult to measure since we have to know the size of the galaxy or cluster before the magnification took place.

In addition, the excess surface density, $\Delta\Sigma$, is even of great importance because it can be measured directly from WL using shear. Cosmic shear is the systematic distortion of images of background galaxies as a result of WL by large-scale objects in the cosmos. Even though $\Delta\Sigma$ is easy to measure, it is rather noisier making it difficult to model than Σ.

The excess surface density, $\Delta\Sigma$, is given as follows.

$$\Delta\Sigma(R) = \bar{\Sigma}(< R) - \Sigma(R), \tag{6}$$

where $\bar{\Sigma}(< R)$ and $\Sigma(R)$ are the mean surface density within a radius, R, and the projected surface density, respectively. Observationally, we can compute $\Delta\Sigma$ directly from WL tangential shear, γ_t, via the following equation.

$$\Delta\Sigma(R) = \bar{\gamma_t}(R)\Sigma_{crit}(z_l, z_s), \tag{7}$$

where z_l and z_s are the redshifts of the lens halo and the source galaxies, respectively. $\bar{\gamma_t}(R)$ represents the average shear (tangential) at a radial distance of R and $\Sigma_{crit}(z_l, z_s)$ is the critical surface density (Sheldon et al.,

2004; Chang et al., 2018; McClintock et al., 2019; Varga et al., 2019; Shin et al., 2021). The tangential shear is a WL signal. It is the tangential component of the ellipticity of the source.

4 Current status of the field

This Section presents the current status of research on dark matter halo density calibration and a summary of findings from the seed papers considered in this synthesis.

4.1 Observations of halo density profiles

We can observe halo density profiles via WL. On the other hand, we can also calibrate density profiles using the number of galaxies per unit area or volume. This method is associated with galaxy formation and evolution and is called the galaxy number density. Another way is to use the number of galaxies per halo of a given mass. This method is a function of mass and is called the Halo Occupation Distribution (Hereafter HOD). The HOD is another method for modeling galaxy number density profiles. Shin et al. (2021) used both WL and HOD to calibrate halo density profiles and found reasonable agreement between the two profiles.

Observational data from astronomical surveys come with several systematic effects. These systematic effects contaminate the data to some extent. Therefore, there is the need to minimize the level of contamination in the data as much as possible to be able to get the best out of it. Currently, there is an active area of research in cosmology on this subject. See (McClintock et al., 2019; Shin et al., 2021) for more details. Research on systematic effects is also geared towards bridging the gap between theory and observations. Bridging this gap will help us make robust predictions that are independent of cosmology. In the Subsections below, we briefly explain some of these systematic effects.

4.1.1 Dilution effect

The dilution effect is due to the uncertainties in distances (photometric redshift errors). Photometric redshift is the redshift estimated using the flux (the magnitude/intensity of light) of galaxies as seen via filters. For details on how to measure photometric redshifts, see redshift on The Dark Energy Survey website.

The dilution effect is the situation where galaxies that do not belong to the source/background sample are mistakenly counted as though they belong to it. This mistake is typically associated with foreground galaxies or galaxies that are at the lens. This leads to underestimation of the WL signal because the misclassified galaxies actually have zero WL signal but are counted as though they have a signal. This leads to contamination of the source sample called the dilution effect. A good practice is to eliminate galaxies that are within a certain range of redshift, Δz, to the lens from the cluster catalog to reduce the extent of the contamination (McClintock et al., 2019; Shin et al., 2021). $\Delta z = 0.1$ in the case of Shin et al. (2021). We can also apply a boost factor to correct the contamination. This helps to calibrate more rigorous estimates of $\Delta\Sigma$ by reducing the contamination due to the dilution effect (Chang et al., 2018; McClintock et al., 2019; Shin et al., 2021). See Chang et al. (2018); McClintock et al. (2019); Shin et al. (2021) for details on boost factor correction techniques.

4.1.2 Miscentering effect

Density profiles are calibrated around halo centers. Therefore, correctly identifying the halo center is very important. Usually, the location of the Brightest Cluster/Central Galaxies (BCGs) is taken to be the halo center. This assumption is good because the central galaxy is the result of lots of mergers, and therefore it is usually the brightest. However, BCGs are not always located at the center of galaxy clusters. A significant fraction of the clusters are sometimes wrongly centered. Therefore, we cannot ignore the effect of the miscentering on WL measurements. A typical downside of miscentering is that the density profile at small radii is severely/badly altered. A good practice is to write the estimated profile by combining the two factions (correctly and wrongly centered clusters) (Chang et al., 2018; McClintock et al., 2019; Shin et al., 2021).

A common question that comes to mind is: How do we know that a halo is miscentered if we do not know its original centers? One way is to compare our cluster centers to those from X-ray measurements because X-ray cluster centers are very accurate. This is because X-ray-selected clusters are independent of redshift and are less affected by systematic effects than optically selected clusters. However, X-ray calibrations are expensive and limited in sample size (Henson et al., 2017). This poses a serious limitation and makes miscentering difficult to handle. Thus, miscentering becomes a major systematic effect to handle.

4.2 Summary of results from seed papers

Table 3 gives a high-level summary of some major themes identified across the four seed papers and what each of them had to say about that theme. For instance, all four seed papers did not consider satellite halos in their analysis for some reason. Diemer & Kravtsov (2014); Shin et al. (2021); Diemer (2022) did not consider satellite halos due to dominant contributions from their host halos. Henson et al. (2017) did not consider satellite halos because they are low-mass halos and their focus is on high-mass halos. See Table 3 below for more themes.

Table 3: Synthesis matrix. This table summarises major themes identified across the four seed papers. A blank space indicates the paper is silent on that theme.

Theme \ **Paper**	**Paper I**	**Paper II**	**Paper III**	**Paper IV**
Inner profile	Reasonably well calibrated by NFW and Einasto fits. Depends on MAR[a] or PH[b]	Not well calibrated by NFW and Einasto fits	Exhibit dependence on two spatial scales - the truncation radius and scale radius	Dominated by baryons towards the center
Outer profile	Depends on MAR or PH	Not well calibrated by 2PT and HOD[c]	Depends on MAR. Dominated by infalling matter	Dark matter dominates at large radii
Splashback feature	Splashback radius, R_{sp}, located at $r \approx R_{200m}$. Steeper in halos with high MAR or PH and vice versa	Location of R_{sp} consistent in WL and galaxy density. Agree with N-body simulations with 20% and 9% uncertainty, respectively	Splashback radius, R_{sp}, is steeper in high-mass halos and occurs faster (at small radii) than in low-mass halos	—
Mass accretion rate and Peak height	Density profiles highly depend on total MAR or PH. The slope at R_{sp} steepens with increasing total MAR or PH	MAR can help us understand halo formation and history of evolution	Density profiles highly depend on total MAR or PH. Slope at R_{sp} steepens with increasing halo mass	—
Scatter in density profiles	Less scatter in the median profile of the inner region and of high PH halos	Less scatter in the density profile of the inner region	Less scatter in the median profile of the inner region and of high-mass halos	Used 16th to 84th percentiles. The width of the scatter looks constant
Halo boundary	Sets R_{vir} as the halo boundary. The DK14 profile is calibrated up to $9R_{vir} \approx 16h^{-1}$Mpc	Sets R_{500c} as halo boundary	Profiles are sensitive to the definition of halo boundary. Sets $R_{200m,all}$ as halo boundary	Sets R_{200m} as halo boundary
NFW and Einasto fit	Do not capture the splashback feature and profile dependence on MAR	Do not capture the splashback feature	Do not capture the splashback feature and profile dependence on MAR	Einasto better than NFW; however, both underestimate cluster masses

[a]Mass Accretion Rate
[b]Peak height
[c]Halo Occupation Distribution

Fig. 3 shows the inner and outer regions of a dark matter halo density profile and the location of the splashback feature. This result is obtained from observational data — from the Atacama Cosmology Telescope (ACT). The halo shown below has a mass of $2.72 \times 10^{14} h^{-1} M_{\odot}$ and the redshift, $z = 0.455$.

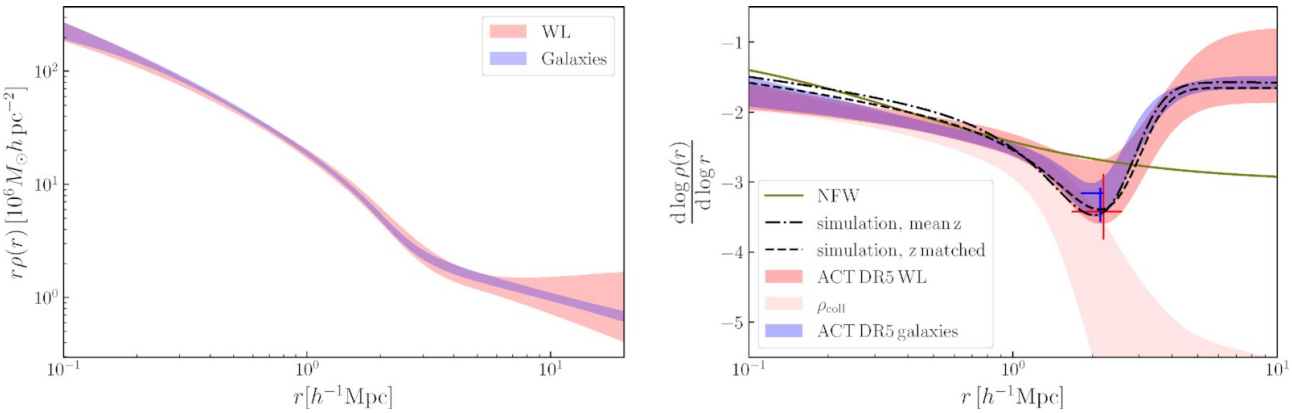

Figure 3: *Left panel:* 3D profiles calibrated from galaxy number density and WL. There is much scatter in the inner region compared to the outer region. Also, the fit of the two methods reasonably agrees with each other. *Right panel:* Logarithmic slope of the density profiles. The NFW profile could not capture the splashback feature and the outer profile. The location of the splashback radius is consistent between the WL estimate (red cross) and that of the galaxy number density estimate (blue cross). We notice from the plot that the truncation in the orbiting term, ρ_{coll}, occurs before the location of the splashback radius. (Credit: Shin et al. (2021))

4.3 Gaps in the literature and future paths

In this Section, we briefly highlight some of the major gaps identified in the literature

- **Poor predictions:** As shown in Fig. 2, analytic models usually result in predictions that do not capture the detailed shape of halo density profiles. Machine learning algorithms have the potential to produce predictions better than those obtained from analytic models.
- **Uncertainty quantification:** Quantifying prediction uncertainty has been a major concern. None of the analytic models in the literature can do this. Given differences in cosmology, it is better to make interval predictions, rather than making single value predictions in the case of the analytic models. Machine Learning ensemble techniques have the potential to achieve this purpose. See Section 5.
- **Halo evolution:** We cannot observe the entire evolution of a ΛCDM halos in a lifetime but we can simulate them. If we simulate the entire time series of a halo's evolution and mass accretion history, then we can predict its mass and density using time series models, such as recurrent neural networks. For instance, we may identify spikes in their mass accretion history that could be informative to us.
- **Splashback feature:** The mass distribution within the splashback feature is still poorly understood. The location of the splashback radius is also poorly understood because it is the result of a complex interaction between the orbiting and infalling matter. Understanding this feature will pave the way for more sophisticated modeling strategies.
- **Low-mass halos:** Most studies impose a mass cut to eliminate low-mass halos from their analysis. This is due to the bias in WL mass estimation for low-mass halos. It is also because the 2-halo term has a significant impact on the mass distribution and density profiles of low-mass halos. Also, low-mass halos have small statistical uncertainties but strong systematic uncertainties. Observationally, low-mass halos are hard to observe. Simulations also have mass limits because low-mass halos have low resolution and strong baryonic effects. In general, it is difficult to tell whether low-mass halos are real clusters or not. Typically, halos of size $\lesssim 10^{12}$ are usually considered low-mass halos. However, the mass limits differ for different studies because the mass limit in halos is dependent on the resolution.

  We suggest binning the data by peak height and then taking representative samples from each bin, instead of entirely eliminating low-mass halos. We believe this will lead to a more robust analysis. In our computing artifact, we binned the data into peak height bins and sampled equally from each bin.
- **Solving observational systematics:** There is no unambiguous way of handling systematic effects. We need more efficient modeling strategies to fill this gap. Simulations can help in this regard. One way is to simulate the systematics and analyze the data as though there are no systematics. If the effect is minimal

then those systematics do not matter a lot and vice versa. This way, we will be able to distinguish between systematics that counts and those that do not count very much. Another way is to introduce systematics into the data and then use simulations to recover them. This will help us test the robustness of existing theories (models and simulations).

- **Contributions from subhalos**: Less attention is given to the contribution of subhalos to their parent halos. Many studies ignore subhalos from their data because they receive dominant contributions from their host halos. However, subhalos account for a portion of the mass in their parent halos and make the density profiles less smooth. This effect is given less attention in the literature. Fielder et al. (2020) presents a possible remedy to exclude the mass associated with subhalos from the total halo mass. This practice smoothens the halo density profile. However, this still needs much attention.

- **Sample sizes:** SZ-selected data, hydrodynamic simulations, and X-ray data are limited in their sample sizes (from a statistical point of view). Thus, it is difficult to tell if conclusions drawn from such studies are significant or just a consequence of the limited sample sizes. Perhaps, more data could lead to more robust results such as the impact of baryons on high-mass halos. Despite this, it is good to state that some incredible results were obtained from such studies.

5 My ongoing research: Neural network methodology

In this Section, we present a machine learning approach to address the first two gaps identified in Section 4.3: That is, to obtain better predictions than analytic models while being able to quantify prediction uncertainty.

Deep neural networks are popular due to their predictive capabilities but quantifying the reliability of their predictions still remains an active area of research. Uncertainty quantification techniques help to measure a model's confidence in its predictions. We expect the measure of uncertainty to be low when the model's level of confidence about its prediction is high and vice versa. In regression base ensemble methods, it is a common practice to use the mean and variance/spread as prediction and measure of uncertainty, respectively. For classification problems, one way is to allow the models in the ensemble to vote and the class with the majority votes wins. Entropy and max-probability are the most popular uncertainty measures for classification ensembles (Durasov et al., 2020). Here, we give a brief description of the ML techniques in this paper. Deep ensembles, Monte Carlo dropout, and Bayesian neural networks are among the most popular uncertainty quantification techniques. However, this paper uses only deep ensembles and Monte Carlo dropout.

The Bayesian neural network offers a framework that is mathematically robust in quantifying model uncertainties but is rather computationally expensive compared to the models adopted in this synthesis. Monte Carlo dropout was introduced as an approximate Bayesian method. Deep ensembles, on the other hand, was introduced as a conceptually simple alternative to the Bayesian neural network (Caldeira & Nord, 2020; Lakshminarayanan et al., 2016; Durasov et al., 2020).

Generally, we expect the aggregate prediction from the ensemble methods to be significantly better than that of any single model or network in isolation. To the author's best knowledge, this paper is novel such that no paper has adopted deep learning models in predicting dark matter halo density profiles.

5.1 Deep ensembles (DEs)

The basic idea is to simply retrain the same neural network architecture many times with random initialization. These random initialization impact the training process and returns several independent models. These models have different sets of weights and biases making them independent; in effect, DEs fits a finite number of independent models. It is possible to add an extra source of randomness by using the bagging or bootstrap aggregation technique. This is simply training each randomly initialized neural network with different subsets of the training data by sampling with replacement from it, but this method has been found to have deteriorating performance (Caldeira & Nord, 2020; Lakshminarayanan et al., 2016; Durasov et al., 2020). DEs is one of the best approaches to quantify model uncertainty; however, it is rather computationally costly to train and evaluate and expensive in terms of memory usage. Thus, DEs is not a suitable candidate for memory-constrained applications. In practice, DEs is also known to have significantly better performance than Monte Carlo dropout in uncertainty quantification tasks with regards to prediction accuracy and error bars; this is attributed to the fact the weight configurations in Monte Carlo dropout results in insufficiently diverse predictions than that of DEs thereby underestimating the resulting error bars (Durasov et al., 2020). DEs is illustrated in Fig. 4.

5.2 Monte Carlo dropout (MCD)

Originally, MCD (or simply dropout) is a regularization technique but this method now serves as a deep learning ensemble technique. The basic idea is to randomly drop a percentage of neurons at each layer for every pass during training (Hinton et al., 2012). However, Gal & Ghahramani (2015) shows that using dropout at inference time is a useful way to quantify prediction uncertainties. They introduce the theoretical and mathematical framework for MCD as approximate Bayesian inference in deep Gaussian processes. Thus, training a dropout network mathematically converges to Bayesian inference. This approximation serves as a useful alternative to Bayesian models. A major factor to consider in MCD is the percentage of neurons to drop. (Gal et al., 2017) focuses on finding the optimal dropout percentages at each layer during training. Srivastava et al. (2014) provides several experimental results and gave some useful heuristics about the dropout technique. They include;

- using a very high dropout rate causes the model to under-learn while a very small dropout rate has little to no effect on the model; hence, a reasonable dropout rate should be in the range 20%-50% with 20% being a reasonable start
- use a reasonably large network
- use dropout on all units/layers
- use large learning rates with decay and high momentum

MCD is a popular and less expensive alternative to DEs but it is rather less reliable as it turns to underestimate the uncertainties. Unlike DEs, MCD uses a correlated set of infinite models. This is because we train a single model, randomly switch off a fraction of nodes and use the resulting models to make predictions. This process can be repeated infinite times. The resulting models are not fully connected neural networks. The models share a fraction of neurons (weights and biases). Thus, MCD trains just a single stochastic network but achieves randomness by randomly eliminating a different set of neurons several times. Doing this during testing results in correlated models. To this end, it becomes possible to make multiple predictions for every data point (Durasov et al., 2020). MCD is illustrated in Fig. 5.

6 Summary and conclusions

Though new physics could potentially help us understand our Universe better, most Cosmologists tend to adopt explanations offered by dark matter theorists because there is very strong evidence of dark matter in the Universe. Vital information useful for understanding cluster cosmology has recently been detected in observations and simulations. Some of these signals are detected around R_{vir} and beyond. Prominent among them is the splashback feature and truncation of the orbiting term. This is becoming a milestone in studies involving dark matter; however, these new discoveries have also created many unanswered questions. Recent studies such as Diemer & Kravtsov (2014); Shin et al. (2021); Diemer (2022) are dedicated to understanding these newly detectable ΛCDM halo properties using various simulated and observational data. The density profiles of the orbiting term have also shown dependence on two important spatial scales — the scale radius, r_s, and the truncation radius, r_t. This is interesting because these two scales depend on different halo properties (r_s depends on the radial definition, R_X, while r_t depends on the total mass accretion rate). This means we cannot accurately model the density profiles with a universal single-scale fitting function like the NFW and Einasto density profiles. Also, density profiles of low-mass halos are significantly affected by the 2-halo term; meanwhile, this has very little to no effect at all on the density profile of high-mass halos because they dominate their environment (Diemer & Kravtsov, 2014; Diemer, 2022). Therefore, we need more efficient models and strategies to account for these factors. We also need to set high-accuracy constraints on existing analytic models to account for these factors.

Diemer & Kravtsov (2014); Diemer (2022) predict halo density profiles as a function of peak height. This is one of the reasons the DK14 profile is gaining much attention. Peak height allows us to estimate redshift-independent density profiles. It also allows for mass comparison across redshift and cosmology. Nonetheless, the dependence of simulations and analytic models on cosmology still remains. Diemer & Kravtsov (2014) also found that density profiles of the inner and outer regions are most self-similar when profiles are rescaled by R_200c and R_200m, respectively. This means that radii defined in reference to the critical density and mean matter density of the universe better describe the inner and outer density profiles, respectively. This also suggests that we need methods to calibrate the two terms with different reference densities.

WL mass calibration is robust compared to other mass calibration methods such as hydrostatic mass calibration for X-ray observations, especially for high-mass halos (McClintock et al., 2019) but we cannot completely rule out the impact of baryons. Previous studies have shown that WL calibrations significantly underestimate cluster masses (Henson et al., 2017; Cromer et al., 2021). However, the bias decreases with respect to increasing mass and tends to approach zero for high-mass halos (Henson et al., 2017). Also, low-mass halos suffer from systematic uncertainties. For these reasons, many studies impose a mass cut on their data to eliminate low-mass halos from their analysis. One way to eliminate this bias is to account for baryonic impact (Cromer et al., 2021). Current findings in the literature show that significant baryonic contributions to low-mass halos have been established. However, we do not know exactly the impact of baryons on high-mass halos. If we do find a significant baryonic impact on high-mass halos, then this will pose serious problems to dark-matter-only mass estimation methods such as WL (Becker & Kravtsov, 2011; Oguri & Hamana, 2011; Henson et al., 2017). However, a major drawback of hydrodynamic simulations is limited sample sizes, especially for high-mass halos (due to computation cost).

Several astronomical surveys are still being conducted with the aim of obtaining high-accuracy cosmology data. Notable among them include the recently launched James Web Space Telescope and the upcoming Vera Rubin Observatory in Chile (expected in 2023), and NASA's Nancy Grace Roman Space Telescope (expected in 2027). All of these are geared toward better understanding our Universe. Some of the previous astronomical surveys include the Dark Energy Survey (DES) (The Dark Energy Survey Collaboration, 2005), the Atacama Cosmology Telescope (ACT) survey (Hilton et al., 2021), and the Sloan Digital Sky Survey (SDSS) (Aihara et al., 2011).

This synthesis also demonstrates the potential of deep neural networks in achieving more accurate density calibration. The methods adopted are capable of estimating prediction uncertainties instead of single-point predictions in the case of the analytic models. We also present a computing artifact available on a public GitHub repository via this link.

Acknowledgements

References

Aihara H., et al., 2011, ApJS, 193, 29

Barnes D. J., Kay S. T., Henson M. A., McCarthy I. G., Schaye J., Jenkins A., 2017, MNRAS, 465, 213

Becker M. R., Kravtsov A. V., 2011, ApJ, 740, 25

Caldeira J., Nord B., 2020, arXiv e-prints, p. arXiv:2004.10710

Chang C., et al., 2018, ApJ, 864, 83

Cromer D., Battaglia N., Miyatake H., Simet M., 2021, arXiv e-prints, p. arXiv:2104.06925

Diemer B., 2022, MNRAS, 513, 573

Diemer B., Kravtsov A. V., 2014, The Astrophysical Journal, 789, 1

Diemer B., More S., Kravtsov A. V., 2013, ApJ, 766, 25

Durasov N., Bagautdinov T., Baque P., Fua P., 2020, arXiv e-prints, p. arXiv:2012.08334

Dutton A. A., Macciò A. V., 2014, Monthly Notices of the Royal Astronomical Society, 441, 3359

Einasto J., 1965, Trudy Astrofizicheskogo Instituta Alma-Ata, 5, 87

Fielder C. E., Mao Y.-Y., Zentner A. R., Newman J. A., Wu H.-Y., Wechsler R. H., 2020, MNRAS, 499, 2426

Gal Y., Ghahramani Z., 2015, arXiv e-prints, p. arXiv:1506.02142

Gal Y., Hron J., Kendall A., 2017, Concrete Dropout, doi:10.48550/ARXIV.1705.07832, `https://arxiv.org/abs/1705.07832`

Gao L., Navarro J. F., Cole S., Frenk C. S., White S. D. M., Springel V., Jenkins A., Neto A. F., 2008, MNRAS, 387, 536

Hayashi E., White S. D. M., 2008, Monthly Notices of the Royal Astronomical Society, 388, 2

Henson M. A., Barnes D. J., Kay S. T., McCarthy I. G., Schaye J., 2017, MNRAS, 465, 3361

Hilton M., et al., 2021, ApJS, 253, 3

Hinton G. E., Srivastava N., Krizhevsky A., Sutskever I., Salakhutdinov R. R., 2012, arXiv e-prints, p. arXiv:1207.0580

Komatsu E., et al., 2011, ApJS, 192, 18

Lakshminarayanan B., Pritzel A., Blundell C., 2016, arXiv e-prints, p. arXiv:1612.01474

Mandelbaum R., Seljak U., Hirata C. M., 2008, J. Cosmology Astropart. Phys., 2008, 006

McCarthy I. G., Schaye J., Bird S., Le Brun A. M. C., 2017, MNRAS, 465, 2936

McClintock T., et al., 2019, MNRAS, 482, 1352

Navarro J. F., Frenk C. S., White S. D. M., 1996, The Astrophysical Journal, 462, 563

Navarro J. F., Frenk C. S., White S. D. M., 1997, The Astrophysical Journal, 490, 493

Nishimichi T., et al., 2019, The Astrophysical Journal, 884, 29

Oguri M., Hamana T., 2011, Monthly Notices of the Royal Astronomical Society, 414, 1851

Planck Collaboration et al., 2014, A&A, 571, A16

Planck Collaboration et al., 2020, A&A, 641, A6

Prada F., Klypin A. A., Simonneau E., Betancort-Rijo J., Patiri S., Gottlober S., Sanchez-Conde M. A., 2006, The Astrophysical Journal, 645, 1001

Salcedo A. N., Wibking B. D., Weinberg D. H., Wu H.-Y., Ferrer D., Eisenstein D., Pinto P., 2019, Monthly Notices of the Royal Astronomical Society, 491, 3061

Sheldon E. S., et al., 2004, AJ, 127, 2544

Shin T., et al., 2019, MNRAS, 487, 2900

Shin T., et al., 2021, Monthly Notices of the Royal Astronomical Society, 507, 5758

Spergel D. N., et al., 2003, ApJS, 148, 175

Springel V., et al., 2005, Nature, 435, 629

Srivastava N., Hinton G., Krizhevsky A., Sutskever I., Salakhutdinov R., 2014, J. Mach. Learn. Res., 15, 1929–1958

Tavio H., Cuesta A. J., Prada F., Klypin A. A., Sanchez-Conde M. A., 2008, arXiv e-prints, p. arXiv:0807.3027

The Dark Energy Survey Collaboration 2005, arXiv e-prints, pp astro–ph/0510346

Varga T. N., et al., 2019, MNRAS, 489, 2511

Fig. 4 illustrates the DEs method. We train a finite set of independent fully connected deep learning models and use them to predict for each data point.

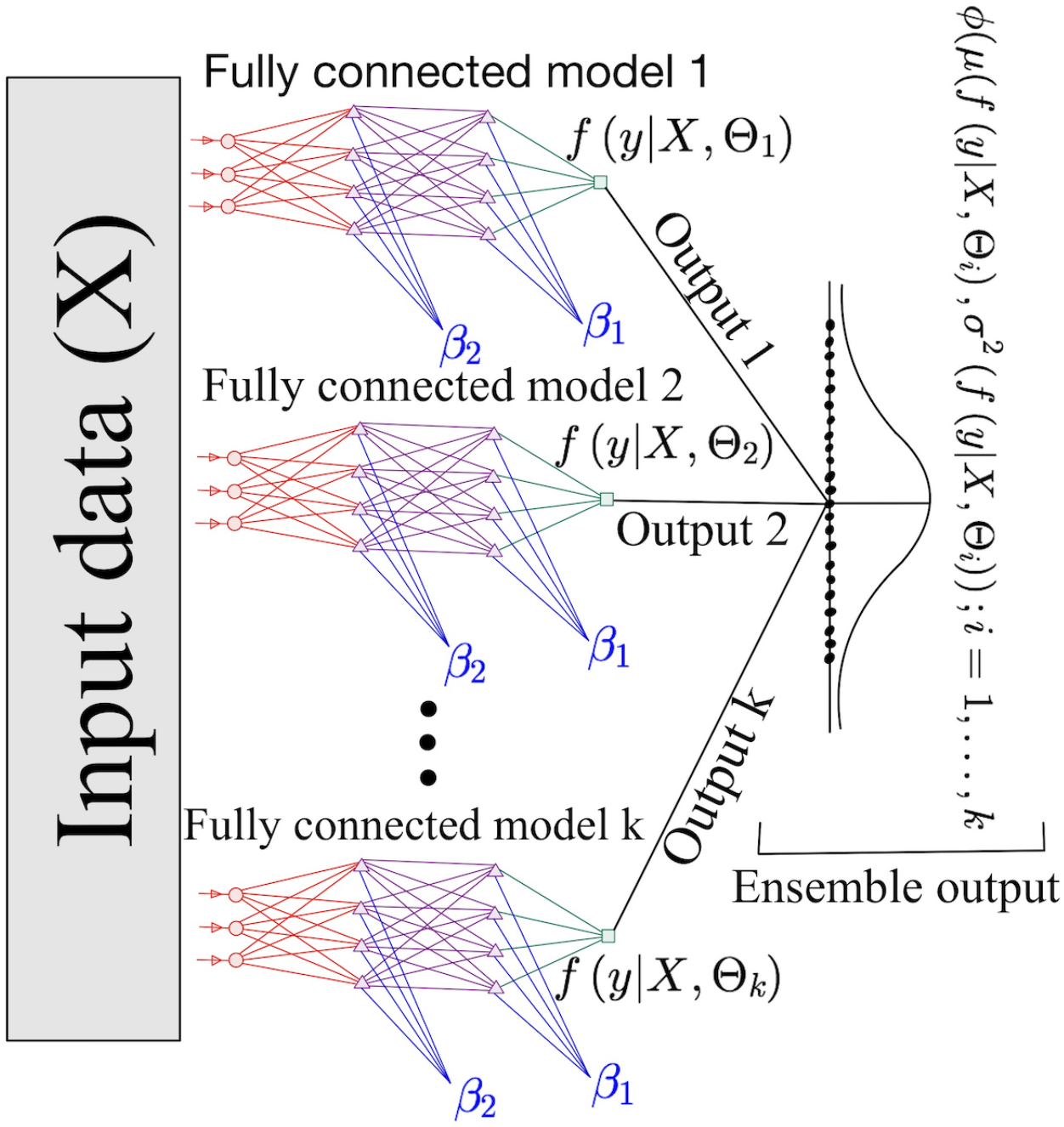

Figure 4: Illustration of DEs. The same neural network architecture is retrained several times with different initializations. This produces independent models with completely non-overlapping (disjoint) parameters. All the models will be used to make predictions. The number of times we train the neural network architecture with different random initialization is the number of independent models we will have. We can only make a finite number of predictions up to the number of models trained. We can form a distribution from all the predictions for a certain observation from which we obtain the aggregate prediction of the ensemble. All models, $f(y|X,\Theta_i); i = 1, 2, \cdots, k$, are completely independent; hence, they do not share any fraction of their parameters/weights, $\Theta_i; i = 1, 2, \cdots, k$.

Fig. 4 illustrates the MCD method. We train a single fully connected deep learning model; however, we can use it to make an infinite number of predictions for each data point.

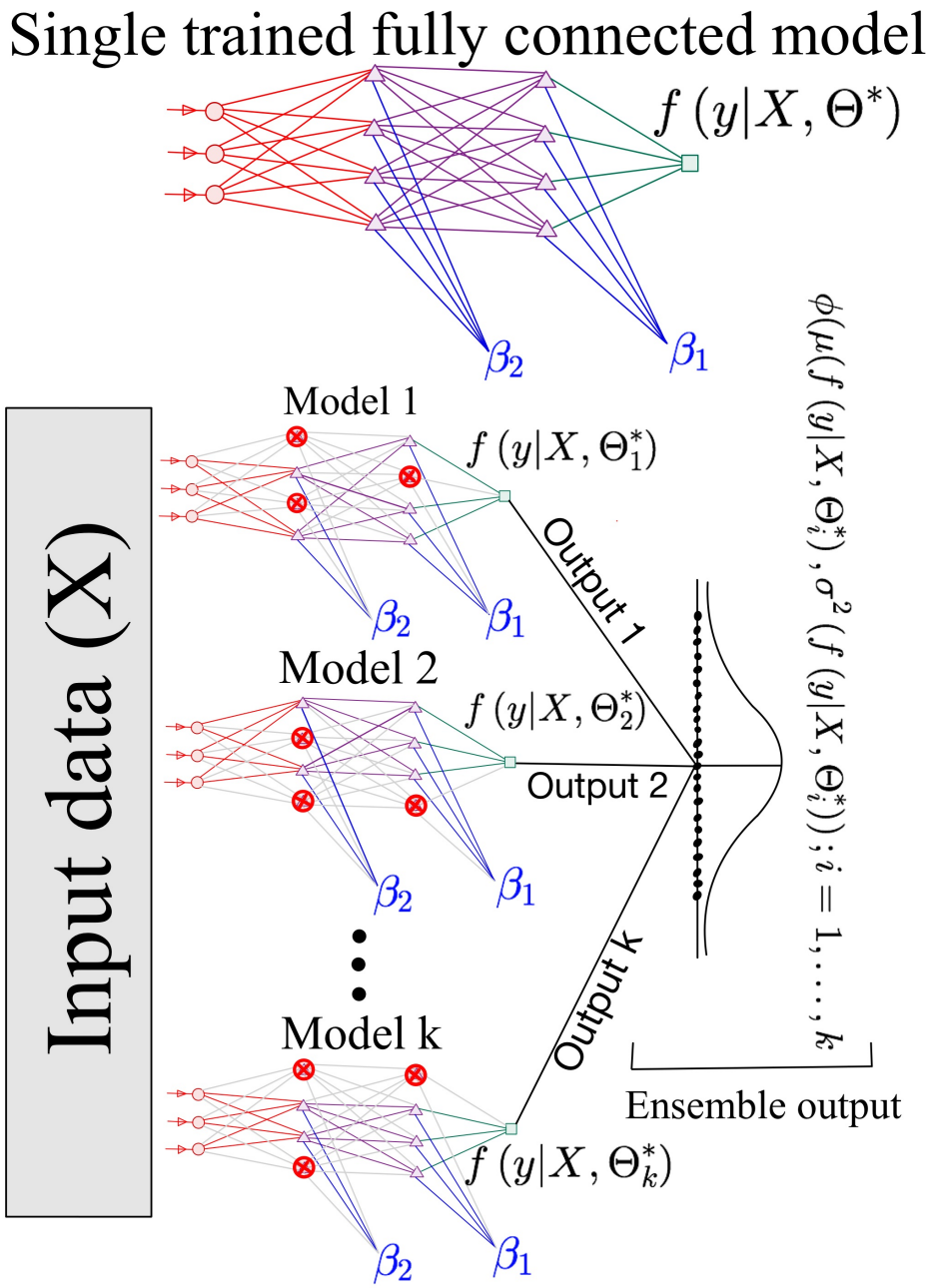

Figure 5: Illustration of MCD. The Figure shows a fully connected neural network model (top) and networks with some nodes switched off (bottom). In this diagram, the red nodes were randomly switched off. Hence, they do not receive any information from the nodes in the previous layer(s). They do not transmit any information to the nodes in the subsequent layer(s) as well. Their contribution is entirely eliminated from the network and this is represented by the gray lines entering or going out from these switched-off nodes. Here, we train a single neural network architecture and then randomly switch off a fraction of the nodes several times and use it to make predictions each time. Thus, we can use the single trained neural network model to make an infinite number of predictions. We can form a distribution from all the predictions for a certain observation from which we obtain the aggregate prediction of the ensemble. MCD results in a correlated set of models. Thus, every two models, $f(y|X,\Theta_i^*), f(y|X,\Theta_j^*); i \neq j; i = 1,2,\cdots,k$, share a fraction of set of their parameters/weights, $\Theta_i^*, \Theta_j^*; i \neq j; i,j = 1,2,\cdots,k$.